Digital in-line holography for biological applications

Wenbo Xu*, M. H. Jericho*, I. A. Meinertzhagen†, and H. J. Kreuzer*‡

*Department of Physics, Dalhousie University, Halifax, NS, Canada B3H 3J5; and †Neuroscience Institute and Department of Psychology, Dalhousie University, Halifax, NS, Canada B3H 4J1

Communicated by John T. Yates, Jr., University of Pittsburgh, Pittsburgh, PA, July 16, 2001 (received for review January 5, 2001)

Digital in-line holography with numerical reconstruction has been developed into a new tool, specifically for biological applications, that routinely achieves both lateral and depth resolution, at least at the micron level, in three-dimensional imaging. The experimental and numerical procedures have been incorporated into a program package with a very fast reconstruction algorithm that is now capable of real-time reconstruction. This capability is demonstrated for diverse objects, such as suspension of microspheres and biological samples (diatom, the head of *Drosophila melanogaster*), and the advantages are discussed by comparing holographic reconstructions with images taken by using conventional compound light microscopy.

Essentially all past and present light microscopy of biological systems has been achieved through the lense of the compound microscope, which yields high spatial resolution at the cost of shallow depth of focus and has, in the process, condemned biological microscopy to a century of histological study made possible only through microtomy. The recent development of confocal microscopy offers an opportunity to image structures in depth within a stack of consecutive two-dimensional (2-D) images, but only for structures that carry some form of fluorescent label. An alternative, in-line holography with spherical waves (1), the simplest realization of the holographic method, has received only limited attention, because reconstruction of the object image with another wave source (light or electron) is not practical. To avoid this problem, various schemes of off-line holography have been devised (2–6), but these lack the essential advantage for microscopy of geometrical enlargement. Another option, numerical reconstruction (7–12), has mostly proved unsatisfactory, however, because of the poor image quality resulting from approximations in the reconstruction algorithm. A recently designed reconstruction algorithm avoids all these approximations, yet it is fast, taking less than a second on a Pentium V computer for an image with 512 × 512 pixels. It yields reconstructed images of the highest lateral and depth resolution (13–15).

In recent years (15–20), we have perfected optical in-line holography with numerical reconstruction, or digital in-line holography (DIH), to the stage at which it has come to represent a new tool for biological applications, supplementing conventional compound light microscopy. The advantages are compelling:

(*i*) Simplicity of the microscope: In-line holography is microscopy without objective lenses. The hardware required is a laser, a pinhole, and a charge-coupled device (CCD) camera.
(*ii*) Simplicity of sample preparation: No sectioning or staining is required, so that living cells can be viewed.
(*iii*) Speed: Changes in the specimen can ultimately be followed at the capture video rate of the CCD chip.
(*iv*) Maximum information: A single hologram contains all the information about the three-dimensional (3-D) structure of the object.
(*v*) Maximum resolution: Optimal resolution, of the order of the wavelength of the laser, can be obtained easily.
(*vi*) Our experimental implementation of DIH, in conjunction with the reconstruction algorithm, essentially eliminates the twin-image problem.

Points *iii–vi* have been examined in detail in earlier papers, in particular in refs. 13 and 21, and will be demonstrated in this note with a number of examples. Prior to this demonstration, we summarize the salient features of DIH and its implementation as an accessory to the compound light microscope.

Principle and Implementation of DIH

We show a schematic of in-line holography in Fig. 1*A*: a laser (L) is directed onto a pinhole (P), having a diameter of the order of the wavelength, which acts as the "point source," from which a spherical wave of wavelength λ emanates. The wave illuminates an object (O) in our setup a few millimeters from the pinhole and forms a geometrically magnified diffraction pattern on a screen (C), in our case a CCD chip, a few centimeters away. If the scattered wave from the object, shown by dotted lines in Fig. 1*A*, is small compared with the unscattered reference wave, the interference pattern on the screen constitutes a hologram, linear in the scattered wave. Typical examples of holograms are given in Fig. 2 *A* and *B*. The hologram is stored as a digital image in a computer. The next step is numerical reconstruction.

The role of reconstruction is to obtain the 3-D structure of the object from the 2-D hologram on the screen or, in physical terms, to reconstruct the wave front at the object. This reconstruction can be achieved via a Kirchhoff–Helmholtz transform[§]

$$K(\mathbf{r}) = \int_S d^2\xi I(\boldsymbol{\xi}) \exp[2\pi i \boldsymbol{\xi}\cdot\mathbf{r}/(\lambda\xi)], \qquad [1]$$

in which the integration extends over the 2-D surface of the screen with coordinates $\boldsymbol{\xi} = (X, Y, L)$, where L is the distance from the source (pinhole) to the center of the screen (CCD chip), and $I(\boldsymbol{\xi})$ is the contrast image (hologram) on the screen obtained by subtracting the images with and without the object present. The function $K(\mathbf{r})$ is significantly structured and different from zero only in the space region occupied by the object. By reconstructing the wave front $K(\mathbf{r})$ on a number of planes at various distances from the source in the vicinity of the object, a 3-D image can be built up from a single 2-D hologram.[¶] The wave front $K(\mathbf{r})$ is a complex function, and one usually plots its magnitude to represent the object, although phase images are also available. For the numerical implementation of the transform, we have developed a fast algorithm that evaluates $K(\mathbf{r})$ with no approximations. It is incorporated in a self-contained

Abbreviations: DIH, digital in-line holography; CCD, charge-coupled device; 2-D, two-dimensional; 3-D, three-dimensional.

‡To whom reprint requests should be addressed. E-mail: kreuzer@is.dal.ca.

§The use of the Kirchhoff–Helmholtz transform for reconstruction was already proposed by Gabor (22); it was also used by Barton (23) and others for the reconstruction of photoelectron holograms, and in Low Energy Electron Diffraction (LEED) holography [see Heinz *et al.* (24)]. It was then applied in Low Energy Electron Point Source (LEEPS) microscopy (13) and used subsequently in optical in-line holography (15–20).

¶In holography, the term "reconstruction" is used to obtain the function $K(\mathbf{r})$ from the hologram. The plot of $|K(\mathbf{r})|$ on a 2-D plane, perpendicular to the optical axis, which we will call a 2-D-holographic reconstruction, is equivalent to one in-focus image taken in a conventional compound microscope. In DIH, one can generate a stack of 2-D holographic reconstructions from a single hologram. Combining such a stack will result in a 3-D image of the object; this latter step is usually referred to as 3-D reconstruction.

The publication costs of this article were defrayed in part by page charge payment. This article must therefore be hereby marked "*advertisement*" in accordance with 18 U.S.C. §1734 solely to indicate this fact.

CELL BIOLOGY

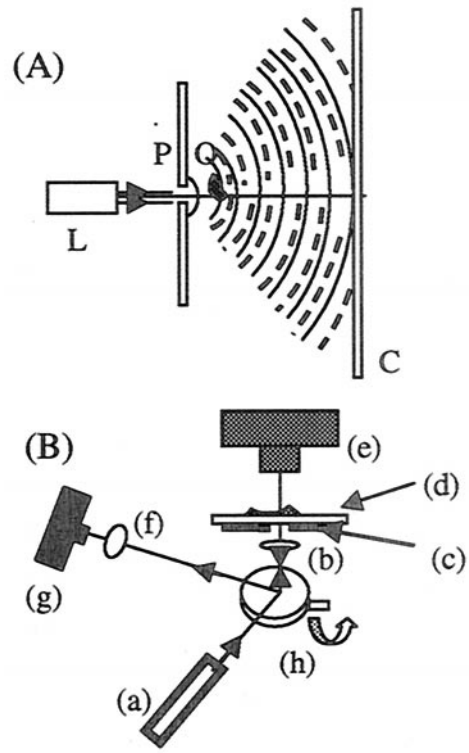

Fig 1. (*A*) Basic arrangement for in-line holography. A laser (L) illuminates a pinhole (P), which acts as a point source. Spherical waves from the pinhole illuminate the object (O), and the interference at the screen (C) of the scattered waves (– – –) with the reference wave (—) constitutes the hologram. (*B*) Schematic of the experimental arrangement used to record an optical image and a hologram of the same object. Eyepiece (f), camera (g), mirror (h), and objective lens (b) are part of an inverted microscope. To record the hologram, light from a laser (a) is reflected off the mirror and focused by the objective lens onto the pinhole (c). The light exiting the pinhole is passed through the object and glass substrate (d) and forms a hologram on the CCD chip (e). To record a conventional optical image of the object, the mirror is turned to allow white light from a lamp (not shown) that illuminates the object to reach a second CCD chip attached to the eyepiece.

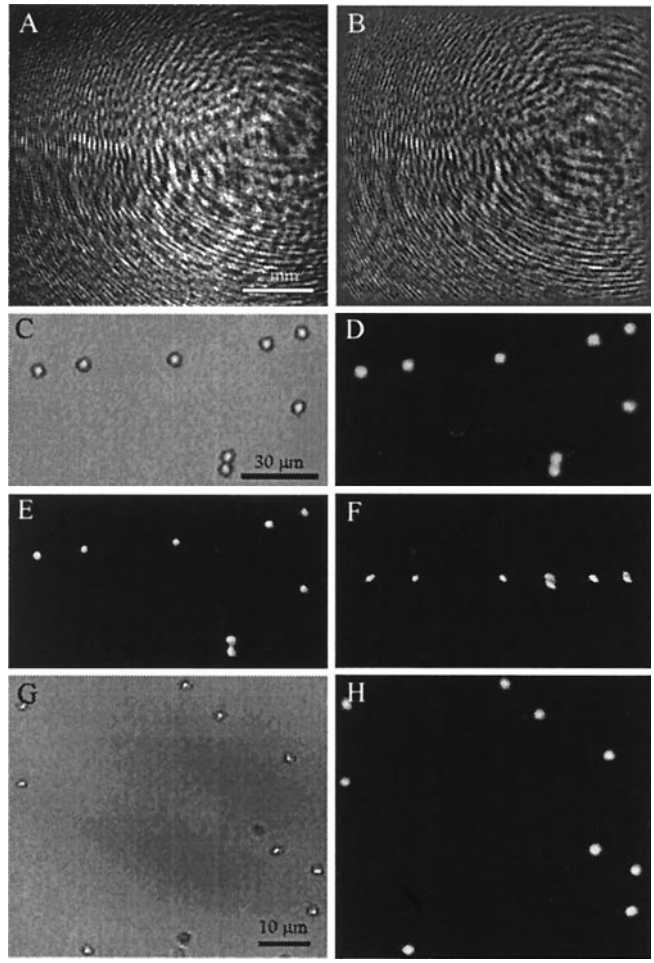

Fig 2. Polymer microspheres (5.13 μm) mounted in gelatin. (*A*) Hologram (1,024 × 1,024 pixels); (*B*) contrast hologram; (*C*) bright-field compound microscope image (Zeiss, ×25/0.80 Plan Neofluar objective); (*D*) holographic 2-D reconstruction in a plane corresponding to *C*; (*E* and *F*) 3-D reconstruction from 15 2-D holographic reconstructions (of which *D* is number 8), by using a software package (AMIRA) (*E*), viewed along the optical axis and (*F*) viewed from below at 90° to the optical axis. Pinhole–object distance, 1.5 mm; pinhole–CCD chip distance, 4.8 cm; green laser (λ = 532 nm), 2-μm pinhole. (*G* and *H*) Polymer microspheres (1.09 μm) mounted in gelatin. (*G*) Bright-field compound microscope image (Zeiss, ×40/0.75 Plan Neofluar objective); (*H*) 2-D holographic reconstruction. Distance of object from pinhole, 0.875 mm; pinhole–CCD chip distance, 3.0 cm; blue laser (λ = 473 nm); 2-μm pinhole.

program package, originally applied to electron holography, called LEEPS, which performs not only the numerical reconstruction but also all other procedures connected with data management and visualization (14).

An important objective for our work was to make detailed comparisons between images from conventional compound light microscopy and those obtained with DIH. For this purpose, the very simple arrangement in Fig. 1*B* was adopted. We used a standard inverted compound microscope (Zeiss Axiovert 25) and obtained a digital record of the bright-field image seen through the ocular in the normal way. To record a hologram of the same sample area, a pinhole (typical diameter 1–5 μm) was placed between the objective lens and the sample, such that the spherical light waves from the pinhole passed through the selected sample area. The laser light that illuminated the pinhole was introduced through a side port in the microscope and directed towards the objective lens and pinhole via a movable mirror. The hologram was recorded with a CCD camera (1,020 × 1,532 pixels, pixel size 9 μm square) that was supported on the microscope work plate and centered over the pinhole and the selected area of the sample. The distance of the CCD camera from the pinhole, typically a few centimeters, was adjusted to capture all interference fringes of the hologram that could be resolved with sufficient pixels. The pinhole was mounted on an X-Y micrometer stage and could be moved out of the way to image the sample in bright-field. This arrangement of the equipment minimized vibrations and also provided an easy method to switch from bright-field to holographic modes of operation.

The object of lateral dimension a to be visualized was placed a distance d, typically a few millimeters from the pinhole, such that the Frauenhofer condition, $a^2 \ll d\lambda$, was fulfilled, to guarantee (*i*) that the image on the screen was dominated by its holographic part, and (*ii*) that twin-image effects in the reconstruction were minimized.

The resolution of the reconstructed images depends on information recorded in the hologram, which, in turn, is limited by the size of the recording CCD chip and its resolution. For a digitally recorded hologram, this resolution is given by the number of pixels, their size and spacing, and the dynamic range of the recorded signals.

From diffraction theory, we know that the resolution of an optical system is given by $a = 0.61\lambda/\sin\vartheta$, where ϑ is half the

opening angle of the divergent beam illuminating the object. To achieve this resolution, we thus need a recording screen of diameter D at a distance L from the source, such that $D/2L > 1/\sqrt{(a/0.61\lambda)^2 - 1}$. This conclusion also follows from inspection of the reconstruction formula, which suggests that two points separated in the object by a distance a will be resolved if their contribution to the interference pattern at the edge of the screen is out of phase, i.e., we have $k\boldsymbol{\xi}\cdot(\mathbf{r} + \mathbf{a})/\xi - k\boldsymbol{\xi}\cdot\mathbf{r}/\xi > 2\pi$. The number of pixels and the dynamics of the CCD chip used for recording the hologram must, of course, resolve the closest diffraction fringes.

As we mentioned above, the input to the reconstruction formula (1) is the contrast image for a perfectly spherical incoming wave. It transpires that perfecting this image is the hardest part of the practical implementation of in-line holography. Guided by experience in photoelectron and LEED holography (23), we have implemented the following procedure:

(*i*) Record digitally the hologram of the object, giving a matrix I_{nm} of the intensity recorded on the CCD chip, where n and m enumerate the pixels in the x and y directions; an example is shown in Fig. 2*A*.
(*ii*) Remove the object and record digitally the intensity matrix $I^{(0)}_{nm}$ of the illuminating laser.
(*iii*) Construct numerically the contrast image, corrected for intensity variations in the primary laser beam. The result is shown in Fig. 2*B*, which, compared with *A*, clearly shows the removal of the overall intensity variation across the laser beam.

By this procedure, almost all imperfections in the laser source are eliminated. Indeed, this step minimizes the quality requirements for the laser itself, so long as the laser is sufficiently stable to capture identically both images. We have checked this fact by comparing the contrast images obtained with (*i*) a high-quality laser and (*ii*) a cheap laser pointer. The results in reconstruction are of comparable quality.

The contrast image is next used in the reconstruction algorithm, based on the transform (1), to produce a series of 2-D holographic reconstructions at different distances from the source, i.e., the pinhole. Because the source–object distance can be measured directly only with an accuracy of a millimeter or so, it is necessary to zoom in with a series of reconstructions at different distances, displayed in the LEEPS program package as a film, to achieve accuracy at the micron level.

Examples

We now present several examples to illustrate the resolution as well as the unique properties of DIH.

A Test: Latex Spheres. Fig. 2 shows images and holograms of latex microspheres having a mean diameter of 5.13 μm. The spheres (refractive index 1.59 at 589 nm) were mounted in a thin layer of gelatin between a microscope slide and a glass coverslip. A hologram, i.e., the intensity matrix I_{nm}, is shown in Fig. 2*A*, taken at a fringe magnification $D/d \gg 33$. To obtain the intensity matrix of the light source, $I^{(0)}_{nm}$, the slide was moved sideways to an area that contained gelatin but no spheres. This reference hologram (not shown), together with the hologram in Fig. 2*A*, was then used to construct the contrast hologram shown in Fig. 2*B*. In Fig. 2*D*, we show a 2-D holographic reconstruction of the spheres taken through the equatorial plane of the spheres. The image clearly resolved all isolated spheres as well as the two spheres that appear to be in direct contact. For comparison, we show in Fig. 2*C* a bright-field compound microscope image.

The power of DIH is that image information is not limited to a plane but is truly 3-D. 2-D holographic reconstructions can thus be performed from a single hologram at a series of selected object depths, and the 3-D reconstruction of the object can be generated from such a stack of 2-D images. In this way, a plan view of the spheres, viewed as if along the optical axis, was obtained by collapsing a stack of 15 consecutive 2-D hologram reconstructions (Fig. 2*E*). That the single hologram in Fig. 2*B* contains the full 3-D structure of the spheres is illustrated in Fig. 2*F*, in which the same stack of 15 reconstructed sections was viewed as if along one axis of the section plane, to provide a side view of the spheres. Viewed from this direction, all spheres lie nearly in the same plane (as the sample geometry requires), and the spheres have again circular profiles. The two spheres that were in contact appear to occupy slightly different positions perpendicular to the sample plane, information that could not be obtained from conventional compound light microscopy (i.e., Fig. 2*C*) alone.

The smallest objects that we so far successfully reconstructed in three dimensions were 1-μm latex spheres (Fig. 2 *G* and *H*). Improvements in our experimental setup should lead to a further gain of a factor of two in x,y resolution.

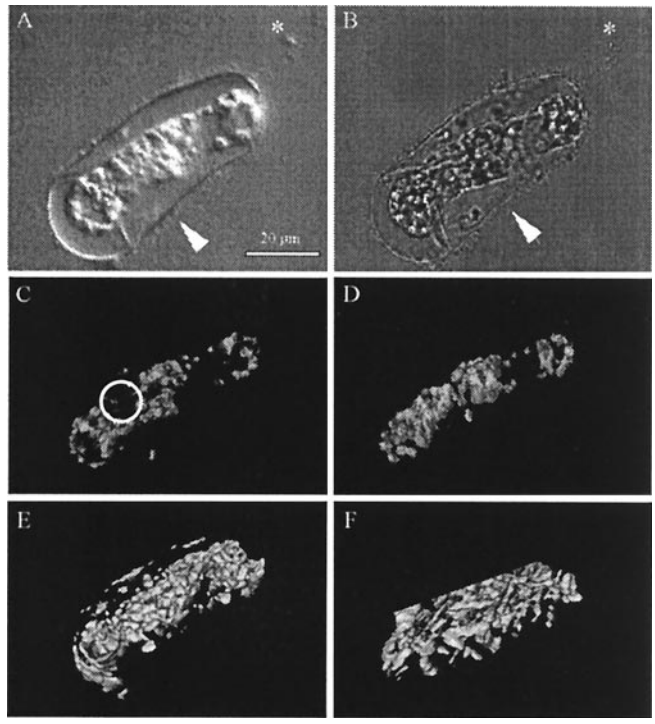

Fig 3. Single cell of *D. brightwellii.* (*A*) Differential interference microscopy obtained with Zeiss Plan Neofluar ×40/0.75 objective and (*B*) a bright-field image obtained in the transmission mode of a confocal microscope with ×40/1.30 oil immersion objective. Note resolution of the outer siliceous frustule (arrowhead) but poor contrast and depth resolution of cell contents in these two images. As a fortuitous marker, a single unidentified bacterium (asterisk) in *A* and *B* is attached to the frustule spine (*B*). (*C* and *D*) 3-D image stack of signal from specimen autofluorescence obtained by LSCM and reconstructed from 23 slices at 1-μm intervals, by using the same specimen and objective as *B*. Note contrast resolution of cell contents and absence of fluorescence in region enclosed by circle. (*C*) Viewed from same direction as in *A* and *B*; (*D*) reconstruction rotated 90° about the cell's long axis from the view in *C*. (*E* and *F*) 3-D reconstruction of the corresponding DIH image stack. (*E*) Same view as *C*, along the optical axis. (*F*) Rotated view, perpendicular to *C*, as in *D*.

Single Cell of *Ditylum brightwellii.* As a second example, we show reconstructed images of a unicellular marine plant cell, the diatom *D. brightwellii*, which was fixed in 4% paraformaldehyde and mounted unstained in gelatin (Fig. 3). Images obtained using DIH (Fig. 3 *E* and *F*) are compared with those either from

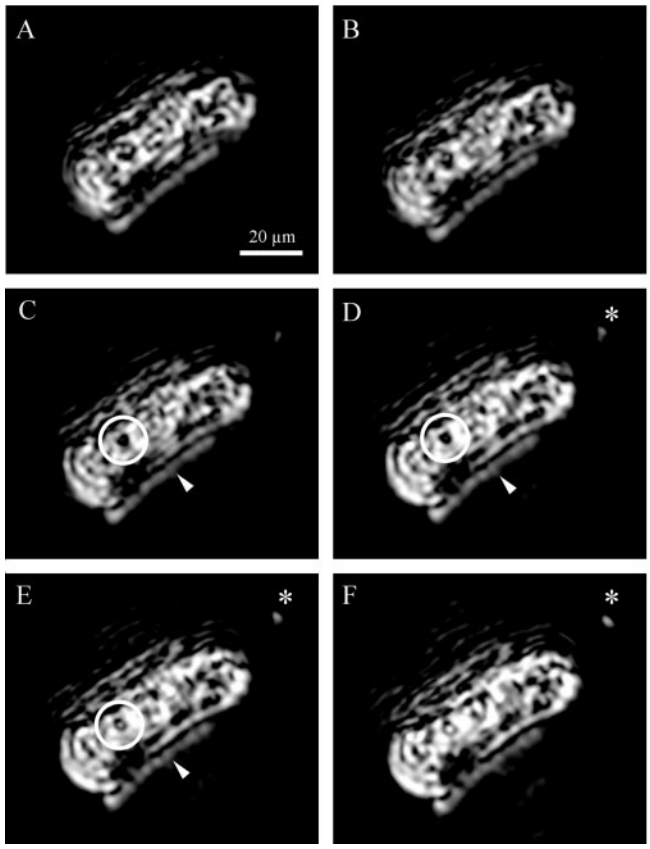

Fig 4. Series of DIH sections at 0.46-μm intervals (sections 18–23 of the 49, from which the 3-D reconstructions in Fig. 3 *E* and *F* were obtained). Note the outline of the frustule (arrowhead in *C–E*), identified by the size position and linear contours of such outlines, and by the similarity between the reconstructed form of the outlines in 3-D and the outline of the frustule in Fig. 3 *A* and *B*. Note also the cavity (circled), a likely vacuole, obscured by the outer portions of the cell in the reconstructed image (Fig. 3 *E* and *F*). The size of the bacterium (asterisk, *D–F*) indicates the resolution attained (see Fig. 3 *A* and *B*). Blue laser, 2-μm pinhole; pinhole-object distance, 1.395 mm; pinhole–CCD chip distance, 3.0 cm.

differential interference (DIC) microscopy by using a conventional compound light microscope (Fig. 3*A*), a bright-field transmitted-light image (Fig. 3*B*), and two views of a stack of images obtained by laser scanning confocal microscopy (LSCM) and reconstructed in 3-D by using software (AMIRA, Konrad Zuse Centrum, Berlin) (Fig. 3 *C* and *D*). Note that all images are shown at the same magnification, by using the same objective; that Fig. 3 *A* and *B* are sections, whereas Fig. 3 *C–F* are 3-D reconstructions; and that the fluorescence images of Fig. 3 *C* and *D*, mostly the cell's chlorophyll-bearing plastids, contain only a subset of the structures imaged by DIH in Fig. 3 *E* and *F*. In particular, the frustule visible in DIC microscopy (Fig. 3*A*) is imaged by DIH but does not appear in LSCM, because it fails to generate a significant fluorescence signal. More complete evaluation of the DIH reconstructions can be made with reference to the original 2-D DIH images (Fig. 4). The cell contains a hollow shell of nonfluorescing cytoplasm, which encloses a vacuole visible in Fig. 3 *C*, also seen in DIH sections (Fig. 4 *C–E*). The sections also reveal the clear outline of the frustule (Fig. 4 *D* and *E*). The frustule does not appear in the 3-D reconstructions (Fig. 3 *E* and *F*), however, because the intensity threshold for the particular reconstructions in Fig. 3 *E* and *F* was chosen instead to reveal the cell's interior and was thus too high to outline the frustule's surface. Nevertheless, this information is contained within the 3-D dataset, which also includes other cytoplasmic organelles.

Head of *Drosophila melanogaster*. DIH can also be used successfully on macroscopic biological specimens, prepared by standard histological procedures, as for a histological section of the head of the fruit fly, *D. melanogaster*. In Fig. 5, the structure of the pigmented compound eye shows high contrast, revealing clear images of its composition by unit ommatidia, one beneath each of the lenslets of the cornea (Fig. 5 *B* and *C*). Different neuropile regions of the brain within the head cuticle are also visible, for example the optic neuropiles underlying the compound eye, although their contrast is somewhat less than for a conventional bright-field image (Fig. 5*A*). Structures are sometimes imaged with slightly different sharpness in the two sections, possibly because the sections are not completely flat.

Resolution Limit

The useful magnification of the diffraction pattern, i.e., the ratio of the source–screen to source–sample distance, is controlled by a number of factors. For high resolution in the reconstructed image, the number of fringes captured by the CCD camera should be as large as possible. For the CCD area that we used (13.8 × 9.2 mm), the resolution criteria discussed above suggest source–screen distances, D, of less than 24 mm for He-Ne gas lasers (λ = 633 nm), less than 29 mm for a green laser (λ = 532 nm), and less than 33 mm for blue lasers (λ = 473 nm). For practical reasons, related to the design of our CCD camera, the source–camera distances we used had to be somewhat larger

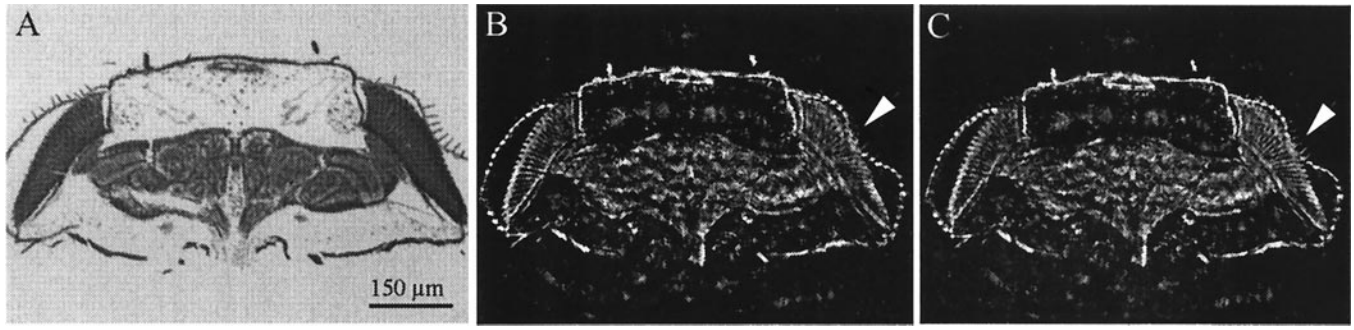

Fig 5. Paraffin wax section, 10 μm thick, of the head of *D. melanogaster*, stained by the Bodian method. (*A*) Bright-field image obtained with conventional compound light microscope (Zeiss Axiophot; objective: ×10/0.3 Plan Neofluar). (*B* and *C*) Two DIH images of the same section as in *A*, by using the same objective, separated by a depth of 6.8 μm. This distance is sufficient to image different bristles over the compound eye, clearer in *C* (arrowhead) than in *B*. The head cuticle (arrowhead, *B*) has high image contrast, but at the contrast level required for DIH, some background material is visible surrounding the specimen. Blue laser; 2-μm pinhole; pinhole–object distance, 6.3 mm; pinhole–CCD chip distance, 6.9 cm.

than the above values. A further degradation of the reconstructed image and hence of the attainable resolution can be caused by the coherence length of the light source. For He-Ne gas lasers, the coherence length is many meters, and the coherence length should not present a problem. For diode lasers and lasers that use second harmonic generation, such as the green and blue lasers used in this study, the line width is considerably broader, and coherence lengths can be only a few millimeters and thus shorter than the source–camera distance. With a blue laser and a line width of 0.1 nm or less, we are confident that holographic reconstructions with a resolution limited only by the wavelength of light can be achieved.

Modern CCD cameras have high sensitivity, and the exposure time even for modest laser power can be short. The exposure times for the holograms presented here were of the order of a few hundred milliseconds. This should make it possible to record video holograms of living cells in three dimensions and their growth and development in the fourth dimension.

Advantages and Future Developments

Our implementation of DIH, even at a stage at which improvements in the hardware are still possible, nevertheless offers a rapid efficient approach to obtain high-contrast 3-D images of biological specimens at fast frame-capture rates. Images are captured digitally, and the ability to reconstruct images at successive selected depths means that image stacks can be collected readily and subsequently reconstructed as entire 3-D datasets. The latter capability has a significant advantage over conventional compound light microscopy that currently can be attained only by using confocal microscopy (LSCM) and then only if the specimen can first be stained with a fluorescent label. With DIH, by contrast, not only is staining unnecessary, even though staining may enhance image contrast, but structures can also be imaged that lack a fluorescence signal. Thus DIH incorporates the advantage of LSCM in providing a digital image stack that can be reconstructed in three dimensions, but it images structures not accessible to LSCM because they lack fluorescence. Compared with other imaging methods, DIH offers additional advantages. It has superior resolution to that currently attained by magnetic resonance microscopy (25). Although lacking the resolution of soft x-ray microscopy (e.g., ref. 26) and high-voltage electron microscopy (e.g., refs. 27, 28), DIH is both simpler and accessible to living cells in thick specimens, for which it therefore offers a prospectively useful correlative method.

Our method can provide the capacity to gather 3-D information at a relatively small additional cost, either as an add-on to an existing compound microscope, enabling successive images to be collected in complementary modes, or as a compact standalone instrument. The availability of the software, LEEPS, offers an advantage to users who may wish to adopt this technology independently.

Future developments may emphasize improved spatial resolution at the submicron level through the adoption of short-wavelength laser light in UV. We have used green and blue laser light to obtain holograms, and the resolution obtained is limited by the number of fringes captured by the light-sensitive CCD chip. Because the number of fringes increases as wavelength shortens, even better resolution can be expected from UV lasers, in which not only is wavelength shorter, but more interference fringes can be recorded. There is no theoretical reason why submicron resolution should not be attainable by using our method, and we predict this development. Experience with in-line holography, in particular photoelectron and LEED holography, indicates that improved z-axis resolution can be obtained by combining holograms at different wavelengths (29–33), an option now practical for DIH through the ready availability of cheap green, blue, and UV lasers.

The interference of waves within a hologram depends sensitively on the phase shifts of the component waves. The method should therefore be of use to image nearly transparent samples, such as those shown in Figs. 4 and 5, in which image contrast is produced by the phase shift between waves arising from different portions of the object.

We thank Ms. Grazyna Tokarczyk and Mr. Harjit Seyan (Neuroscience Institute, Dalhousie University) for providing the specimens. This work was supported by grants from the National Sciences and Engineering Research Council of Canada.

1. Gabor, D. (1948) *Nature (London)* **161,** 777–778.
2. Leith E. N. & Upatnieks, J. (1962) *J. Opt. Soc. Am.* **52,** 1123–1130.
3. Leith, E. N. & Upatnieks, J. (1963) *J. Opt. Soc. Am.* **53,** 1377.
4. Leith, E. N. & Upatnieks, J. (1964) *J. Opt. Soc. Am.* **54,** 1295–1301.
5. Kreis, T. (1996) *Holographic Interferometry* (Akademie, Berlin).
6. Hariharan, P. (1996) *Optical Holography* (Cambridge Univ. Press, Cambridge, U.K.).
7. Aoki, Y. (1970) *IEEE Trans. Audio Electroacoust.* **18,** 258.
8. Kronrod, M. A., Yaroslavski, L. P. & Merzlyakov, N. S. (1972) *Sov. Phys.-Tech. Phys. (USA)* **17,** 329–333.
9. Demetrakopoulos, T. H. & Mittra, R. (1974) *Appl. Opt.* **13,** 665–670.
10. Onural, L. & Scott, P. D. (1987) *Opt. Eng.* **26,** 1124–1132.
11. Liu, G. & Scott, P. D. (1987) *J. Opt. Soc. Am. A* **4,** 159–165.
12. Onural, L. & Oezgen, M. T. (1992) *J. Opt. Soc. Am. A* **9,** 252–260.
13. Kreuzer, H. J., Nakamura, K., Wierzbicki, A., Fink, H.-W. & Schmid, H. (1992) *Ultramicroscopy* **45,** 381–403.
14. Kreuzer, H. J. & Pawlitzek, R. P. (1993–1998) LEEPS Ver. 1.2 (Helix Science Applications, Halifax, NS, Canada).
15. Kreuzer, H. J., Fink, H.-W., Schmid, H. & Bonev, S. (1995) *J. Microsc.* **178,** 191–197.
16. Schmid, H., Fink, H.-W. & Kreuzer, H. J. (1995) *J. Vac. Sci. Technol. B* **13,** 2428–2431.
17. Kreuzer, H. J. (1995) *Micron* **26,** 503–509.
18. Kreuzer, H. J. & Pawlitzek, R. A. (1996) in *Simulation and Experiment in Laser Metrology*, Proceedings of the International Symposium on Laser Applications in Precision Measurements, Balatonfüred, Hungary, June 3–6, 1996, eds. Füzessy, Z., Jüptner, W. & Osten, W. (Akademie, Berlin).
19. Kreuzer, H. J. & Pawlitzek, R. A. (1997) in *Fringe '97:* Proceedings of the 3rd International Workshop on Automatic Processing of Fringe Patterns, Bremen, Germany, September 15–17, 1997, eds. Jüptner, W. & Osten, W. (Akademie, Berlin).
20. Kreuzer, H. J., Pomerleau, N., Blagrave, K. & Jericho, M. H. (1999) *SPIE* **3744,** 65–74.
21. Gölzhäuser, A., Völkel, B., Grunze, B. & Kreuzer, H. J. (2001) *Micron*, in press.
22. Gabor, D. (1949) *Proc. R. Soc. London Ser. A* **197,** 454–487.
23. Barton, J. J. (1988) *Phys. Rev. Lett.* **61,** 1356–1359.
24. Heinz, K., Starke, U. & Bernardt, J. (2000) *Prog. Surf. Sci.* **64,** 163–178.
25. Jasanoff, A., Meister, M. & Cory, D. G. (2000) *Soc. Neurosci. Abstr.* **26,** 2123.
26. Meyer-Ilse, W., Hamamoto, D., Nair, A., Lelievre, S. A., Denbeaux, G., Johnson, L., Pearson, A. L., Yager, D., Legros, M. A. & Larabell, C. A. (2001) *J. Microsc.* **201,** 395–403.
27. Hama, K., Arii, T. & Ito, Y. (2000) *J. Electron Microsc.* **49,** 1–4.
28. Martone, M. E., Deerinck, T. J., Yamada, N., Bushong, E. & Ellisman, M. H. (2000) *J. Histotechnol.* **23,** 261–270.
29. Harp, G. R., Saldin, D. K. & Tonner, B. P. (1990) *Phys. Rev. Lett.* **65,** 1012–1015.
30. Wei, C. M., Zhao, T. C. & Tong, S. Y. (1990) *Phys. Rev. Lett.* **65,** 2278–2281.
31. Tong, S. Y., Hua, L. & Huang, H. (1990) *Phys. Rev. Lett.* **67,** 3102–3105.
32. Saldin, D. K., Reuter, K., de Andres, P. L., Wedler, H., Chen, X., Pendry, J. B. & Heinz, K. (1996) *Phys. Rev. B* **54,** 8172–8177.
33. Shegelski, M. R. A., Faltus, S., Clark, T. & Kreuzer, H. J. (1998) *Ultramicroscopy* **74,** 169–178.